

Interfacial Symmetry Control of Emergent Ferromagnetism at the Nanoscale

A. J. Grutter,^{*,†} A. Vailionis,[†] J. A. Borchers,[‡] B. J. Kirby,[‡] C. L. Flint,[†] C. He,[§]
E. Arenholz,^{||} and Y. Suzuki[†]

[†]*Geballe Laboratory for Advanced Materials, Stanford University, Stanford, CA 94305*

[‡]*NIST Center for Neutron Research, National Institute of Standards and Technology,
Gaithersburg, MD, 20899*

[¶]*Department of Materials Science and Engineering, Stanford University, Stanford, CA
94305*

[§]*Department of Materials Science and Engineering, University of California, Berkeley, CA
94720*

^{||} *Advanced Light Source, Lawrence Berkeley National Lab, Berkeley, CA 94720*

[⊥]*Department of Applied Physics, Stanford University, Stanford, CA 94305*

E-mail: alexander.grutter@nist.gov

Abstract

The emergence of complex new ground states at interfaces has been identified as one of the most promising routes to highly tunable nanoscale materials. Despite recent progress, isolating and controlling the underlying mechanisms behind these emergent properties remains among the most challenging materials physics problems to date. In particular, generating ferromagnetism localized at the interface of two non-ferromagnetic materials is of fundamental and technological interest. Moreover, the ability to turn the ferromagnetism on and off would shed light on the origin of such emergent phenomena and is promising for spintronic applications. We demonstrate that ferromagnetism confined within one unit cell at the interface of CaRuO₃ and CaMnO₃ can be switched on and off by changing the symmetry of the oxygen octahedra connectivity at the boundary. Interfaces which are symmetry-matched across the boundary exhibit interfacial CaMnO₃ ferromagnetism while the ferromagnetism at symmetry-mismatched interfaces is suppressed. We attribute the suppression of ferromagnetic order to a reduction

in charge transfer at symmetry-mismatched interfaces, where frustrated bonding weakens the orbital overlap. Thus interfacial symmetry is a new route to control emergent ferromagnetism in materials such as CaMnO₃ which exhibit antiferromagnetism in bulk form.

Keywords

magnetism, perovskite, interfacial properties, superlattice, charge transfer, interfacial symmetry

The discovery of novel electronic and magnetic ground states in ABO₃ perovskite oxide heterostructures has been made possible through control of thin film synthesis at nanometer length scales.¹⁻⁷ Discontinuities in band structure, valence states, or interaction lengths at interfaces give rise to novel behavior confined near the interface. More recently, systematic tuning of the atomic structure by manipulating BO₆ octahedral connectivity has opened up new pathways for generating emergent phenomena in perovskite heterostructures.^{8,9} The manipulation of octahe-

dral connectivity can be achieved through epitaxial strain, superlattice periodicity modulation, and introducing crystallographic symmetry (mis)match at the interfaces. For example, ferroelectricity has been predicted in perovskite superlattices where neither constituent material is ferroelectric.^{9,10} In ferromagnetic systems such as $\text{La}_{0.7}\text{Sr}_{0.3}\text{MnO}_3/\text{Eu}_{0.7}\text{Sr}_{0.3}\text{MnO}_3$, $\text{LaMnO}_3/\text{SrTiO}_3$, or $\text{La}_{0.7}\text{Sr}_{0.3}\text{MnO}_3$, the magnetic properties are tunable through interfacial MnO_6 octahedral tilt and rotation.^{11–14}

Although octahedral connectivity control is typically used analogously to strain and pressure application,^{11–14} emergent magnetic interfaces present opportunities to realize effects which truly have no bulk analog. In a system with pure interfacial ferromagnetism, such as LaMnO_3 or CaMnO_3 -based superlattices, the impact of these structural variations may be amplified to produce large changes in the magnetism.^{3,4,15–20} Even more dramatically, completely switching the interfacial ferromagnetic order on and off may be possible.

$\text{CaRuO}_3/\text{CaMnO}_3$ is an ideal model system composed of an antiferromagnetic insulator (CaMnO_3) and a paramagnetic metal (CaRuO_3) where emergent interfacial ferromagnetism has been investigated.^{4,5,19–22} Nanda et al. attributed the ferromagnetism to double exchange interactions among interfacial Mn ions mediated by itinerant electrons transferred from the adjacent CaRuO_3 .²⁰ This charge transfer has been observed through electron energy loss spectroscopy, and density functional theory calculations show that competition between antiferromagnetic superexchange and ferromagnetic double exchange stabilizes a canted ferromagnetic state with a magnetization of $0.85\text{--}1.0 \mu_B/\text{Mn}$ within the first unit cell.^{19,20}

In this letter, we demonstrate for the first time the ability to switch emergent ferromagnetism on and off through control of octahedral connectivity. More specifically, crystallographic symmetry-mismatch across the interfaces, associated with incommensurate tilt and rotation of the MnO_6 and RuO_6 octahedra, can modulate and even entirely suppress the interfacial ferromagnetism residing within a single unit cell of the CaMnO_3 layer. Our results indicate that

the creation of discontinuities in the interfacial structural symmetry inhibits electron transfer from CaRuO_3 to CaMnO_3 , destabilizing the ferromagnetism and illustrating the power of controlling charge transfer at interfaces.

We systematically probed the magnetic and atomic structure of $((\text{CaRuO}_3)_n/(\text{CaMnO}_3)_m)_{10}$ superlattices, designated (n/m) , grown on (001) oriented SrTiO_3 across the range $n = 2\text{--}4$ and $m = 3\text{--}19$.¹⁹ In bulk, both materials are isostructural and possess orthorhombic unit cells with $Pbnm$ symmetry doubling the pseudocubic perovskite unit cell.^{23,24} Unless otherwise noted, we refer to the CaRuO_3 and CaMnO_3 pseudo-cubic structure and lattice parameters of 0.386 nm and 0.373 nm , respectively. References to the orthorhombic system are designated with a subscripted O .

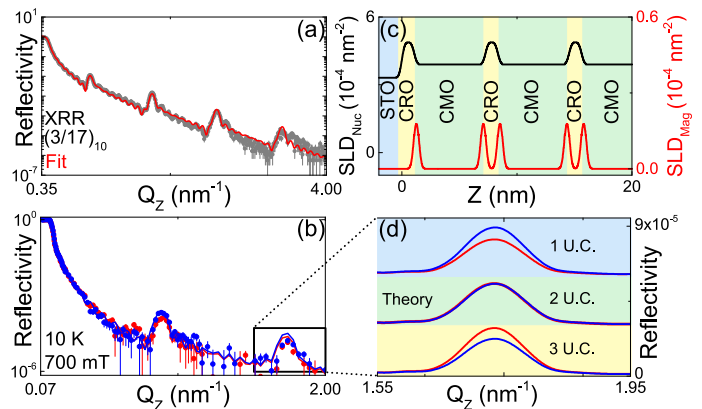


Figure 1: (a) XRR of a (3/17) superlattice with theoretical fit. (b) PNR and fit for spin-up (blue) and spin-down (red) neutrons. The spin-up (blue) reflectivity has higher intensity at the second order Bragg peak. (c) Nuclear (black) and magnetic (red) depth profile associated with the fit shown. (d) Theoretical reflectivity at the second order Bragg peak for interfacial ferromagnetic layer thicknesses of 1-3 unit cells. Error bars correspond to ± 1 standard deviation.

X-ray reflectivity (XRR) and polarized neutron reflectometry (PNR) (Figure 1) reveal uniform superlattices, individual layers within 0.7% of designed thicknesses, and interfacial roughnesses of 0.5 nm . These techniques probe several nonlocal sources of roughness, such as long-range thickness variation. Locally, even

smoother interfaces are expected, in agreement with our scanning transmission electron microscopy (STEM) measurements.¹⁹

Having established structural quality, we probed the magnetic depth profile using PNR measurements of (3/10), (3/11), (3/17), (3/18), and (4/19) superlattices using the PBR beamline at the NIST Center for Neutron Research (NCNR). Figure 1b shows neutron spin-up and spin-down reflectivities for the (3/17) superlattice along with the reflectivity calculated from a model (Figure 1c) composed of 10 uniform stacked layers of CaRuO₃ and CaMnO₃ with a single unit cell of ferromagnetic CaMnO₃ at each interface.^{22,25} The spin-splitting near the critical edge and first Bragg peak is sensitive to the magnitude of the magnetization and is consistent with SQUID magnetometry. In contrast, the second order peak provides sensitivity to ferromagnetic layer thickness, illustrated in Figure 1d. Models of the (3/17) superlattice with ferromagnetic layer thicknesses of 1, 2, and 3 unit cells predict a 28%, -1%, and -26% splitting between spin-up and spin-down reflectivities at the second order Bragg peak, respectively. The observed second order Bragg peak splitting for the (3/17) sample is 46(±26)%, favoring a single unit cell of ferromagnetism. Similar results are obtained for the (3/18) and (4/19) samples. Together, all results give greater than a 99.4% confidence that the ferromagnetic layer is confined to a single unit cell of CaMnO₃ at the interface and conclusively rule out thicknesses exceeding 2 unit cells.

SQUID magnetometry (Figure 2a) indicates the coexistence of interfacial ferromagnetic and interior antiferromagnetic CaMnO₃ layers, through the shift of the magnetization loops after cooling in ±5 T. The shift is a manifestation of exchange bias which results from exchange coupling between the ferromagnetic and adjacent antiferromagnetic layer. Exchange bias is observed below 70 K for all periodicities and increases linearly with CaMnO₃ thickness throughout the measured range.^{19,22} Figure 2a also shows the typical temperature dependence of the magnetization revealing a T_C of 100(3) K for the interfacial ferromagnetic CaMnO₃ lay-

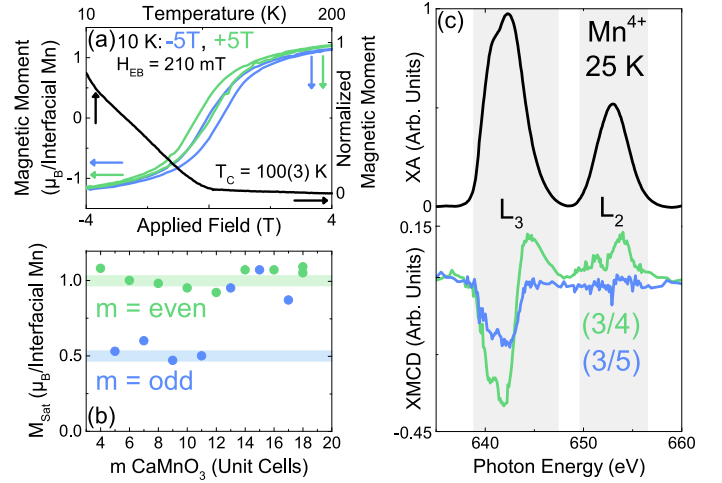


Figure 2: (a) Field dependence of the magnetization for a (3/18) superlattice. Temperature dependence of the magnetization when increasing the superlattice temperature in applied fields of 10 mT after field-cooling in 5 T. (b) Interfacial M_{Sat} for (3/ m) superlattices with $4 \leq m \leq 18$. (c) (top) Mn $L_{3,2}$ XA spectra of a typical (3/4) superlattice. (bottom) Mn $L_{3,2}$ XMCD for a (3/4) and (3/5) sample.

ers. Plotting saturation magnetization (M_{Sat}) for (3/ m) as function of CaMnO₃ thickness (Figure 2b), reveals a modulation from 0.5 to 1.0 μ_B/Mn (normalized by the number of interfacial Mn sites) with CaMnO₃ layer thickness. Once $m \geq 12$, M_{Sat} of all samples converges to 1.0 μ_B/Mn . Element specific magnetic characterization using X-ray absorption (XA) and XMCD in total electron yield (TEY) mode were performed at beamlines 6.3.1 and 4.0.2 of the Advanced Light Source and are shown in Figure 2c. They confirmed the magnetometry measurements, i.e. superlattices with “ $m = \text{even}$ ” number of CaMnO₃ layers exhibit significantly larger dichroism on the Mn $L_{3,2}$ absorption edge than superlattices with “ $m = \text{odd}$ ” number of CaMnO₃ layers.

The variation in M_{Sat} for $m < 12$ (Figure 2b) is commensurate with the periodicity of the orthorhombically distorted perovskite unit cell – double that of the pseudo-cubic unit cell. That is, superlattices with an even number of pseudocubic CaMnO₃ unit cells per layer ($m = \text{even}$) exhibit significantly larger magnetization than “ $m = \text{odd}$ ” superlattices. Thus, to un-

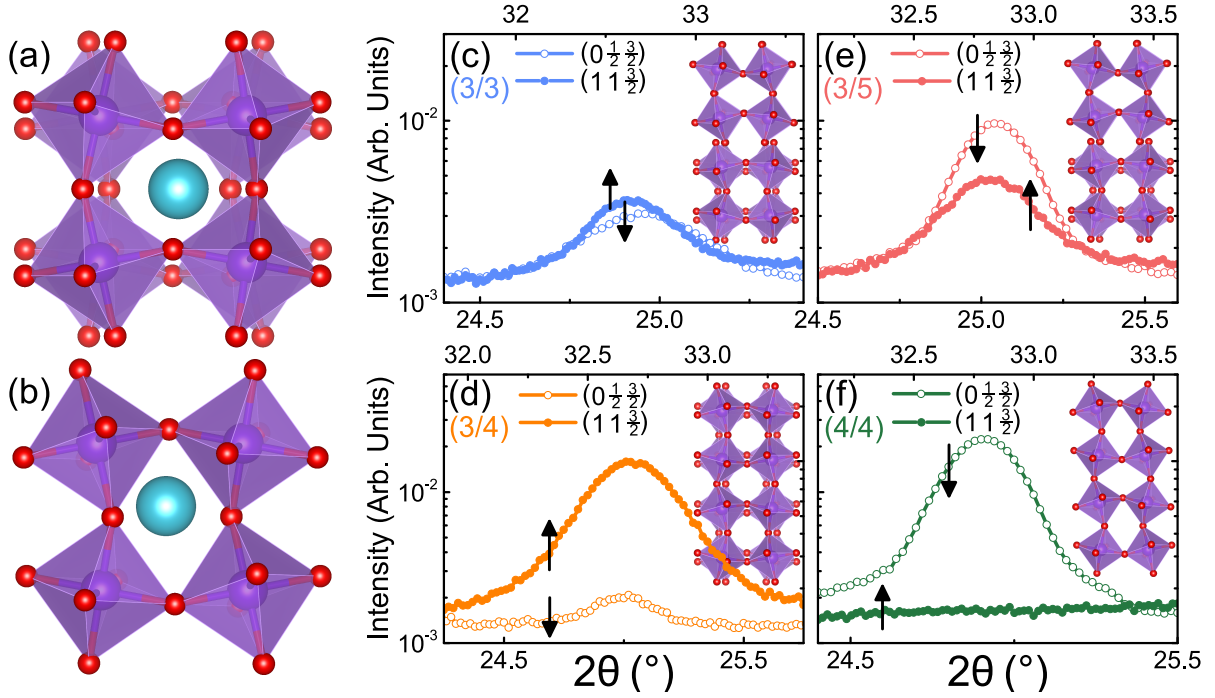


Figure 3: Schematic of (a) $[110]_O$ and (b) $[001]_O$ domains in CaRuO_3 and CaMnO_3 , viewed along the film growth axis.²⁶ Raw intensity of the $(0\frac{1}{2}\frac{3}{2})$ and $(11\frac{3}{2})$ XRD peaks for a (c) (3/3), (d) (3/4), (e) (3/5), and (f) (4/4) superlattice. The black arrows indicate whether the peak shown is associated with the top or bottom x-axis. Schematics show an in-plane view of the expected symmetries present in each superlattice. In these schematics, the growth axis is parallel to the y-axis of the plot.

Understand the underlying mechanism behind the M_{Sat} modulation with CaMnO_3 layer thickness, we performed detailed structural studies of the interfaces using x-ray diffraction at beamline 7-2 of the Stanford Synchrotron Radiation Laboratory.

The orthorhombic distortion symmetry may have either out-of-phase or in-phase rotations of the oxygen octahedra when viewed along the growth axis, giving rise to $[110]_O$ (Figure 3a) and $[001]_O$ (Figure 3b) oriented orthorhombic domains respectively. The alignment of the $[110]_O$ or $[001]_O$ directions along the growth axis is indicated by the presence of the $(210)_O$ or $(203)_O$ diffraction peaks, corresponding to $(0\frac{1}{2}\frac{3}{2})$ and $(11\frac{3}{2})$ peaks respectively. The presence or absence of these two peaks enables identification of the orthorhombic domains present in our superlattices.²² Figures 3c-3f show the relative intensities of the $(0\frac{1}{2}\frac{3}{2})$ and $(11\frac{3}{2})$ peaks for a representative subset of superlattices with $m < 6$. All possible super-

lattice periodicity combinations, (even/even), (odd/even), (even/odd), and (odd/odd), were studied. We find that (even/even) superlattices are $[110]_O$ out-of-plane dominant while (odd/even) superlattices are $[001]_O$ out-of-plane dominant. Superlattices with (even/odd) and (odd/odd) are in a mixed state, with moderate intensities in both $(0\frac{1}{2}\frac{3}{2})$ and $(11\frac{3}{2})$ peaks. Examining the entire thickness range revealed that the $(0\frac{1}{2}\frac{3}{2})$ intensity grows rapidly with increasing CaMnO_3 thickness, implying that the bulk of the CaMnO_3 is $[110]_O$ oriented. In contrast, the $(11\frac{3}{2})$ peak does not scale with CaMnO_3 thickness, suggesting sensitivity to changes in domain orientation near the interfaces.²²

Figure 4 shows the dependence of M_{Sat} on the $(11\frac{3}{2})$ peak intensity (probing domains in the $[001]_O$ orientation). All samples collapse onto a universal curve in which a moderate $(11\frac{3}{2})$ peak intensity is associated with a sharp reduction in magnetization. Further, after accounting for the aforementioned $(0\frac{1}{2}\frac{3}{2})$ intensity dependence

on CaMnO_3 thickness, we find that the $(0\frac{1}{2}\frac{3}{2})$ peak is most intense for (even/even) samples, modest in (odd/odd) and (even/odd) samples and smallest for (odd/even) samples.²² Thus, a mixture of $[001]_O$ and $[110]_O$ domains at the interface results in lower magnetization while the presence of a dominant domain orientation (either $[001]_O$ or $[110]_O$ domains) at the interface results in higher magnetization.

Mixed domain states occur only in superlattices with an odd number of pseudocubic CaMnO_3 unit cells per layer, and may be indicative of one of several structural configurations: crystallographic symmetry-mismatch across all interfaces, crystallographic symmetry-mismatch across every other interface, or crystallographic symmetry-matched interfaces with equal populations of the two orthorhombic domain types. However, symmetry-matched interfaces would not differentiate samples with even and odd CaMnO_3 layers with respect to magnetization. If the reduced magnetization results from interfacial symmetry-mismatch, then the sharp switching of magnetization between (n/m) and $(n/m+1)$ samples can be explained in terms of complete suppression of ferromagnetism through symmetry-mismatch at half of the interfaces. For this configuration, in which ferromagnetism is suppressed at half of the interfaces, the depth dependence of our XMCD results requires that $\text{CaMnO}_3/\text{CaRuO}_3$ be the nonmagnetic interface while the $\text{CaRuO}_3/\text{CaMnO}_3$ interface is magnetic.²² This interpretation is consistent with SQUID magnetometry, PNR, and XMCD data.

For superlattices with an even number of pseudocubic CaMnO_3 unit cells per layer, there is a dominant orthorhombic domain orientation and each interface is symmetry-matched. With interfacial symmetry matching, we expect strong interfacial bonding which enables charge transfer and emergent ferromagnetism. Therefore although the two cases do not have the same symmetry, both (even/even) and (odd/even) superlattices exhibit higher magnetization. Specifically, (even/even) superlattices exhibit majority $[110]_O$ domains regardless of CaRuO_3 layer thickness, while (odd/even) su-

perlattices are majority $[001]_O$. This suggests that the structural distortions in CaRuO_3 and its surface termination play a role in determining the emergent ferromagnetic behavior.

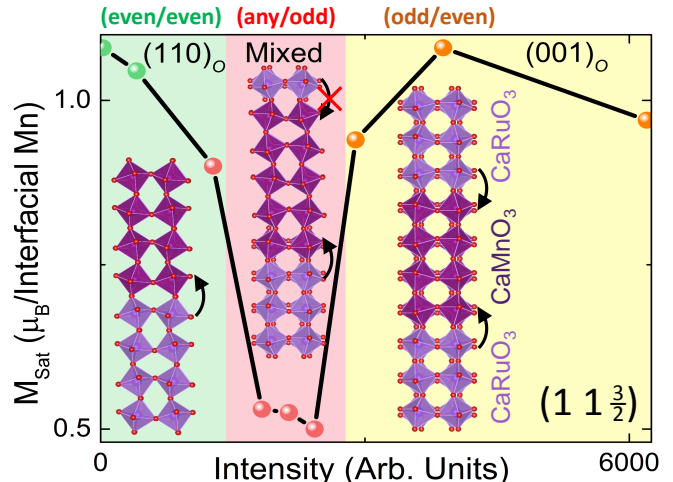


Figure 4: M_{Sat} vs. integrated $(11\frac{3}{2})$ peak intensity. (even/even) samples in green and (odd/even) samples in yellow exhibit high magnetization, while (odd/odd) and (even/odd) samples (i.e., $m = \text{odd}$) in red have suppressed magnetization.

The observed correlation between orthorhombic growth domains and M_{Sat} demonstrates that interfacial ferromagnetism can be tuned effectively through lattice distortions and interfacial crystallographic symmetry (mis)match. We propose that this symmetry-mismatch occurs at half of the interfaces in superlattices with an odd number of CaMnO_3 unit cells per superlattice layer, altering the Ru-O-Mn bonding in a way which reduces orbital overlap. We postulate that the symmetry-mismatch and reduced orbital overlap suppresses electron transfer at half the interfaces, stabilizing purely antiferromagnetic interactions and reducing the overall ferromagnetic moment.²² Thus modification of the superlattice periodicity by only a single unit cell dramatically changes both the interfacial symmetry and the resultant magnetic order.

In summary, we have demonstrated that interfacial ferromagnetism can be tuned and even suppressed through interfacial crystallographic symmetry-mismatch. Although octahedral tilting and rotations are typically secondary ef-

fects, in the present case the extreme sensitivity of the interfacial ferromagnetism to modification of the electron transfer enables the octahedral superstructure to play a major role. In contrast to past examples which were complicated by strain and thickness variation, the fully interfacial nature of the magnetism in isostructural $\text{CaRuO}_3/\text{CaMnO}_3$ superlattices along with the oscillatory thickness dependence provides a truly unambiguous demonstration of the power of octahedral connectivity on the magnetic ground state. These observations unveil new approaches towards designing emergent magnetic order and reveal a system in which there is a delicate balance of exchange interactions that result in abrupt switching between ferromagnetic and antiferromagnetic order. Although further theoretical investigation is warranted, it is clear that octahedral connectivity plays a critical role in tuning magnetism at the nanometer length scale. Such tunability is promising for future incorporation of these oxide interface systems into spintronic applications.

Acknowledgement This work was supported by the U.S. Department of Energy, Office of Basic Energy Sciences, Division of Materials Sciences and Engineering under Award No. DESC0008505. Use of the Stanford Synchrotron Radiation Light source, SLAC National Accelerator Laboratory, is supported by the U.S. Department of Energy, Office of Science, Office of Basic Energy Sciences under Contract No. DE-AC02-76SF00515. The Advanced Light Source is supported by the Director, Office of Science, Office of Basic Energy Sciences, of the U.S. Department of Energy under Contract No. DE-AC02-05CH11231. Polarized neutron reflectivity and neutron diffraction was performed at the NIST Center for Neutron Research (supported by the U.S. Department of Commerce). We thank Dr. L. Harriger, Dr. W. Ratcliff II, Dr. D. Parshall, Dr. S. Watson, Dr. R. Erwin, and Dr. W. Chen for assistance with the neutron diffraction and Dr. M. Stiles for fruitful discussions.

Supporting Information Available

Additional information is available regarding the methods, instrumentation, X-ray absorption spectroscopy analysis, X-ray diffraction, and neutron diffraction. This material is available free of charge via the Internet at <http://pubs.acs.org>.

Notes

The authors declare no competing financial interest.

References

- (1) Ohtomo, A. and Hwang, H. Y., *Nature* **427**, 423 (2004)
- (2) Ueda, K., Tabata, H., and Kawai, T., *Science* **280**, 1064 (1998)
- (3) Gibert, M., Zubko, P., Scherwitzl, R., Íñiguez, J., and Triscone, J.-M., *Nat. Mater.* **11**, 195 (2012)
- (4) Takahashi, K. S., Kawasaki, M., and Tokura, Y., *Appl. Phys. Lett.* **79**, 1324 (2001)
- (5) Freeland, J. W., Chakhalian, J., Boris, A. V., Tonnerre, J.-M., Kavich, J. J., Yordanov, P., Grenier, S., Zschack, P., Karapetrova, E., Popovich, P., Lee, H. N., and Keimer, B., *Phys. Rev. B* **81** 094414 (2010)
- (6) Grutter, A. J., Yang, H., Kirby, B. J., Fitzsimmons, M. R., Aguiar, J. A., Browning, N. D., Jenkins, C. A., Arenholz, E., Mehta, V. V., Alaan, U. S., and Suzuki, Y., *Phys. Rev. Lett.* **111**, 087202 (2013)
- (7) Lee, J.-S., Xie, Y. W., Sato, H. K., Bell, C., Hikita, Y., Hwang, H. Y., and Kao, C.-C., *Nat. Mater.* **12**, 703 (2013)
- (8) He, J., Borisevich, A., Kalinin, S. V., Pennycook, S. J., and Pantelides, S. T. *Phys. Rev. Lett.* **105**, 227203 (2010)
- (9) Rondinelli, J. M., May, S. J., and Freeland, J. W., *MRS Bull.* **37**, 261 (2012)

- (10) Rondinelli, J. M. and Fennie, C. J., *Adv. Mater.* **24**, 1961 (2012)
- (11) Moon, E. J., Colby, R., Wang, Q., Karapetrova, E., Schlepütz, C. M., Fitzsimmons, M. R., and May, S. J., *Nature Communications* **5**, 5710 (2014)
- (12) Zhai, X., Cheng, L., Liu, Y., Schlepütz, C. M., Dong, S., Li, H., Zhang, X., Chu, S., Zheng, L., Zhang, J., Zhao, A., Hong, H., Bhattacharya, A., Eckstein, J. N., and Zeng, C., *Nat. Commun.* **5** 4283 (2014)
- (13) Moon, E. J., Balachandran, P. V., Kirby, B. J., Keavney, D. J., Sichel-Tissot, R. J., Schlepütz, C. M., Karapetrova, E., Cheng, X. M., Rondinelli, J. M., and May, S. J., *Nano Lett.* **14**, 2509 (2014)
- (14) Liao, Z., Huijben, M., Zhong, Z., Gauquelin, N., Macke, S., Green, R. J., Van Aert, S., Verbeeck, J., Van Tendeloo, G., Held, K., Sawatzky, G. A., Koster, G., and Rijnders, G., *Nat. Mater.* **15**, 425 (2016)
- (15) May, S. J., Shah, A. B., te Velthuis, S. G. E., Fitzsimmons, M. R., Zuo, J. M., Zhai, X., Eckstein, J. N., Bader, S. D., and Bhattacharya, A. *Phys. Rev. B* **77**, 174409 (2008)
- (16) Bhattacharya, A., May, S. J., te Velthuis, S. G. E., Warusawithana, M., Zhai, X., Jiang, B., Zuo, J.-M., Fitzsimmons, M. R., Bader, S. D., and Eckstein, J. N., *Phys. Rev. Lett.* **100**, 257203 (2008)
- (17) Hoffman, J., Tung, I. C., Nelson-Cheeseman, B. B., Liu, M., Freeland, J. W., and Bhattacharya, A., *Phys. Rev. B* **88**, 144411
- (18) Chakhalian, J., Freeland, J. W., Srajer, G., Stremper, J., Khaliullin, G., Cezar, J. C., Charlton, T., Dalglish, R., Bernhard, C., Cristiani, G., Habermeier, H.-U., and Keimer, B., *Nat. Phys.* **2**, 244 (2006)
- (19) He, C., Grutter, A. J., Gu, M., Browning, N. D., Takamura, Y., Kirby, B. J., Borchers, J. A., Kim, J. W., Fitzsimmons, M. R., Zhai, X., Mehta, V. V., Wong, F. J., and Suzuki, Y., *Phys. Rev. Lett.* **109**, 197202 (2012)
- (20) Nanda, B. R. K., Satpathy, S., and Springborg, M. S., *Phys. Rev. Lett.* **98** 216804 (2007)
- (21) Grutter, A.J., Kirby, B.J., Gray, M.T., Flint, C.L., Alaan, U.S., Suzuki, Y., and Borchers, J. A., *Phys. Rev. Lett.* **115**, 047601 (2015)
- (22) See Supplemental Material at [URL will be inserted by publisher] for additional details regarding the methods, instrumentation, X-ray absorption spectroscopy analysis, X-ray diffraction, and neutron diffraction. This material is available free of charge via the Internet at <http://pubs.acs.org>.
- (23) Kojitani, H., Yuichi, S., and Masaki, A. *Phys. Earth Planet. Inter.* **165**, 127 (2007)
- (24) Paszkowicza, W., Piętosa, J., Woodley, S. M., Dłużewska, P. A., Kozłowski M., and Martin, C., *Powder Diffr.* **25**, 46 (2010)
- (25) Kirby, B. J., Kienzle, P. A., Maranville, B. B., Berk, N. F., Krycka, J., Heinrich, F., and Majkrzak, C.F., *Curr. Opin. Colloid Interface Sci.* **17**, 44 (2012)
- (26) Momma, K., and Izumi, F., *J. Appl. Crystallogr.*, **44**, 1272 (2011)